INTERNATIONAL JOURNAL FOR NUMERICAL METHODS IN FLUIDS
Int. J. Numer. Meth. Fluids 2006; **52**:1293–1313
Published online 25 April 2006 in Wiley InterScience (www.interscience.wiley.com). DOI: 10.1002/fld.1221

Development of a class of multiple time-stepping schemes for convection–diffusion equations in two dimensions

R. K. Lin[‡,§] and Tony W. H. Sheu[*,†,¶]

Department of Engineering Science and Ocean Engineering, National Taiwan University, No. 1, Sec. 4, Roosevelt Road, Taipei, 106 Taiwan, Republic of China

SUMMARY

In this paper we present a class of semi-discretization finite difference schemes for solving the transient convection–diffusion equation in two dimensions. The distinct feature of these scheme developments is to transform the unsteady convection–diffusion (CD) equation to the inhomogeneous steady convection–diffusion-reaction (CDR) equation after using different time-stepping schemes for the time derivative term. For the sake of saving memory, the alternating direction implicit scheme of Peaceman and Rachford is employed so that all calculations can be carried out within the one-dimensional framework. For the sake of increasing accuracy, the exact solution for the one-dimensional CDR equation is employed in the development of each scheme. Therefore, the numerical error is attributed primarily to the temporal approximation for the one-dimensional problem. Development of the proposed time-stepping schemes is rooted in the Taylor series expansion. All higher-order time derivatives are replaced with spatial derivatives through use of the model differential equation under investigation. Spatial derivatives with orders higher than two are not taken into account for retaining the linear production term in the convection–diffusion-reaction differential system. The proposed schemes with second, third and fourth temporal accuracy orders have been theoretically explored by conducting Fourier and dispersion analyses and numerically validated by solving three test problems with analytic solutions. Copyright © 2006 John Wiley & Sons, Ltd.

KEY WORDS: convection–diffusion; convection–diffusion-reaction; alternating direction implicit; time-stepping schemes

1. INTRODUCTION

The objective of this paper is to develop a class of finite difference schemes for solving the physically important convection–diffusion scalar transport equation, which is the simplest

*Correspondence to: Tony W. H. Sheu, Department of Engineering Science and Ocean Engineering, National Taiwan University, No. 1, Sec. 4, Roosevelt Road, Taipei, 106 Taiwan, Republic of China.
†E-mail: twhsheu@ntu.edu.tw
‡E-mail: d89525003@ntu.edu.tw
§Postdoctoral Researcher.
¶Professor.

Contract/grant sponsor: National Science Council; contract/grant number: NSC 92-2611-E-002-008

Received 21 May 2004
Revised 17 January 2006
Accepted 18 January 2006

prototype fluid dynamics/heat transfer equation. This equation is also computationally important since it is often chosen to benchmark the proposed numerical schemes. Prediction of this working equation is, thus, a subject of considerable significance for several decades. In the present study we restrict our attention to the two-dimensional unsteady case.

A reliable transport scheme requires suppressing convective instabilities and retaining prediction accuracy when convective terms largely dominate diffusive terms in the equation [1]. It has been known that use of stable multi-dimensional schemes may contaminate the solutions with excessive diffusion error. A highly accurate scheme, on the other hand, suffers from instability problem which may even cause solutions to diverge. The main theme of the present study is to construct a time-evolving convection–diffusion scheme which accommodates high accuracy and good stability properties concurrently. Numerical simulation of partial differential equations is also concerned with numerical efficiency, thus we do not regard a scheme as useful if it is not cost-effective.

The rest of this paper is organized as follows. Section 2 presents the time-dependent convection–diffusion equation in a domain of two dimensions. This is followed by the presented semi-discretization finite-difference schemes and the alternating direction implicit solution procedures. Our emphasis is on the development of schemes which can provide higher temporal and spatial accuracy, while retaining stability. In Section 3 we present several temporal discretization schemes and in Section 4 the method of approximating spatial derivatives. Theoretical studies of the proposed temporal schemes are given in Section 5. Section 6 presents numerical results for purposes of validating the methods. In Section 7, we give concluding remarks.

2. WORKING EQUATION AND SOLUTION ALGORITHM

We consider in this paper the following two-dimensional equation for a passive scalar ϕ transported in the domain Ω:

$$\phi_t + u\,\phi_x + v\,\phi_y - k(\phi_{xx} + \phi_{yy}) = 0 \tag{1}$$

We shall in what follows assume that the velocity components (u and v) and the diffusion coefficient k are constant. The above equation together with the initial condition $\phi(x, y, 0)$ and the boundary condition $\phi = g$ on $\partial\Omega$ constitute a closed initial boundary-valued problem.

For purposes of computational efficiency in solving the multi-dimensional equation, we apply the alternating direction implicit (ADI) scheme of Peaceman and Rachford [2]. Use of this spatial operator splitting strategy enables us to calculate solutions iteratively through the two steps given below:

Predictor step:

$$\phi_t^* + u\phi_x^* - k\phi_{xx}^* = -v\phi_y^n + k\phi_{yy}^n \tag{2}$$

Corrector step:

$$\phi_t^{n+1} + v\phi_y^{n+1} - k\ \phi_{yy}^{n+1} = -u\phi_x^* + k\phi_{xx}^* \tag{3}$$

Take the unsteady convection–diffusion equation (2) as an example. Application of the first-order accurate forward difference scheme for ϕ_t^* yields the inhomogeneous convection–diffusion-reaction equation given by $u\phi_x^* - k\phi_{xx}^* + (1/\Delta t)\phi^* = -v\phi_y^n + k\phi_{yy}^n + (1/\Delta t)\phi^n$. How

accurately the employed scheme can approximate the inhomogeneous convection–diffusion-reaction equation turns out to be the key issue in solving Equation (1). With this recognition in mind, the equation worthy of consideration is chosen to be

$$\phi_t + u\phi_x - k\phi_{xx} = f \tag{4}$$

where $f(\equiv -v\phi_y^n + k\phi_{yy}^n)$ is a known value, which is obtained from ϕ at $t = n\Delta t$.

3. TEMPORAL DISCRETIZATION METHODS

The building block in developing the parabolic finite-difference scheme for the model equation (4) involves approximating the time derivative term and then the remaining spatial derivatives. Within this semi-discretization framework, ϕ_t is approximated by the following Taylor series expansion of ϕ with respect to time at $t = n\Delta t$:

$$\phi^{n+1} = \phi^n + \Delta t\phi_t^n + \frac{(\Delta t)^2}{2!}\phi_{tt}^n + \frac{(\Delta t)^3}{3!}\phi_{ttt}^n + \frac{(\Delta t)^4}{4!}\phi_{tttt}^n + \cdots + \text{HOT} \tag{5}$$

The temporal accuracy of the discretization varies according to the number of truncated terms shown on the right-hand side of (5).

3.1. One-step second-order temporal scheme

Considering the following approximation for Equation (5):

$$\phi^{n+1} = \phi^n + \Delta t\phi_t^n + \frac{(\Delta t)^2}{2}\phi_{tt}^n \tag{6}$$

The expression for ϕ_t^n in (6) can be directly obtained from Equation (4) as

$$\phi_t^n = f^n - u\phi_x^n + k\phi_{xx}^n \tag{7}$$

As for ϕ_{tt}^n, it could be replaced with the spatial derivatives from the equation that is derived by performing $\partial/\partial t$ on Equation (4). This is, however, undesirable since the introduced dispersion term ϕ_{xxx} may destabilize the discrete equation. To circumvent this difficulty, we avoid invoking the terms like ϕ_{xxx} and ϕ_{xxxx} by employing

$$\phi_{tt}^n = \frac{2}{(\Delta t)^2}(\phi^{n+1} - \phi^n - \Delta t\phi_t^n) = \left(\frac{\phi^{n+1} - \phi^n}{\Delta t}\right)_t + \text{CT} \tag{8}$$

where the correction term CT is written as

$$\text{CT} = \frac{2}{(\Delta t)^2}(\phi^{n+1} - \phi^n) - \frac{1}{\Delta t}(\phi_t^{n+1} + \phi_t^n) \tag{9}$$

Substitution of Equation (7) for ϕ_t^n and Equations (8)–(9) for ϕ_{tt}^n into Equation (6) enables us to derive the following convection–diffusion-reaction equation:

$$\overline{u}\phi_x^{n+1} - \overline{k}\phi_{xx}^{n+1} + 2\phi^{n+1} = \overline{F} \tag{10}$$

where $\overline{F} = \overline{f}^{n+1} + 2\phi^n + (\overline{f}^n - \overline{u}\phi_x^n + \overline{k}\phi_{xx}^n) + (\Delta t)^2\text{CT}$ and $(\overline{u}, \overline{k}, \overline{f}) = (u\Delta t, k\Delta t, f\Delta t)$. Note that Equation (7) at the time level $n+1$ is required to derive the above equation. Upon

obtaining the updated value of ϕ, one can compute ϕ_t^{n+1} from $f^{n+1} - u\phi_x^{n+1} + k\phi_{xx}^{n+1}$ using the high-order spatial scheme described in Section 4. The solution ϕ^{n+1} for (10) is obtained iteratively for $\overline{f}^{n+1}$ until the user's specified tolerance is reached.

3.2. Multi-step higher-order temporal schemes

3.2.1. Two-step third-order temporal scheme. The scheme described in Section 3.1 can be refined by taking $((\Delta t)^3/6)\phi_{ttt}^n$ into consideration. Inclusion of this term into the scheme development for improving temporal accuracy is accomplished by virtue of the following two-step time-stepping method. In the first step, the solution advancing one-third of the time increment Δt is approximated as

$$\phi^{n+(1/3)} = \phi^n + \frac{\Delta t}{3}\phi_t^n + \frac{(\Delta t)^2}{18}\phi_{tt}^n \tag{11}$$

This is followed by introducing a parameter A in the representation of ϕ_t^n as

$$\phi_t^n = \frac{\phi^{n+1} - \phi^n}{\Delta t} + A\Delta t\phi_{tt}^{n+(1/3)} \tag{12}$$

Substitution of Equation (11) into (12) can render

$$\phi^{n+1} = \phi^n + \Delta t\phi_t^n + \frac{(\Delta t)^2}{2!}\phi_{tt}^n + \frac{(\Delta t)^3}{3!}\phi_{ttt}^n + \cdots$$

on condition that $A = \frac{1}{2}$. Therefore, the third-order temporal accuracy can be obtained from the following two-step time-stepping scheme:

$$\phi^{n+(1/3)} = \phi^n + \frac{\Delta t}{3}\phi_t^n + \frac{(\Delta t)^2}{18}\phi_{tt}^n \tag{13a}$$

$$\phi^{n+1} = \phi^n + \Delta t\phi_t^n + \frac{(\Delta t)^2}{2}\phi_{tt}^{n+(1/3)} \tag{13b}$$

Following the same procedures as those described in Section 3.1, the third-order temporally accurate solution can be obtained from the following two CDR partial differential equations:

$$\overline{u}\phi_x^{n+(1/3)} - \overline{k}\phi_{xx}^{n+(1/3)} + 6\phi^{n+(1/3)} = \overline{f}^{n+(1/3)} + 6\phi^n + (\overline{f}^n - \overline{u}\phi_x^n + \overline{k}\phi_{xx}^n) + \frac{(\Delta t)^2}{3}\mathrm{CT}_1 \tag{14a}$$

$$\begin{aligned}\overline{u}\phi_x^{n+1} - \overline{k}\phi_{xx}^{n+1} + \frac{4}{3}\phi^{n+1} = {} & \overline{f}^{n+1} + \frac{4}{3}\phi^n + \frac{4}{3}(\overline{f}^n - \overline{u}\phi_x^n + \overline{k}\phi_{xx}^n) \\ & - (\overline{f}^{n+(1/3)} - \overline{u}\phi_x^{n+(1/3)} + \overline{k}\phi_{xx}^{n+(1/3)}) + \frac{2(\Delta t)^2}{3}\mathrm{CT}_2\end{aligned} \tag{14b}$$

Two correction terms CT_i $(i = 1, 2)$ shown above are written as

$$\mathrm{CT}_1 = \frac{18}{(\Delta t)^2}(\phi^{n+(1/3)} - \phi^n) - \frac{3}{\Delta t}(\phi_t^{n+(1/3)} + \phi_t^n)$$

$$\mathrm{CT}_2 = \frac{2}{(\Delta t)^2}(\phi^{n+1} - \phi^n) - \frac{3}{2\Delta t}(\phi_t^{n+1} - \phi_t^{n+(1/3)}) - \frac{2}{\Delta t}\phi_t^n$$

3.2.2. Three-step fourth-order temporal scheme. The scheme can be further improved by increasing one order of temporal accuracy using the following three-step time-stepping algorithm:

$$\phi^{n+(1/3)} = \phi^n + \frac{\Delta t}{3}\phi_t^n + \frac{\Delta t^2}{18}\ \phi_{tt}^n \tag{15a}$$

$$\phi^{n+(2/3)} = \phi^n + \frac{2\Delta t}{3}\phi_t^n + \frac{2\Delta t^2}{9}\phi_{tt}^n \tag{15b}$$

$$\phi^{n+1} = \phi^n + \Delta t(\alpha\phi_t^n + \beta\phi_t^{n+(1/3)} + \gamma\phi_t^{n+(2/3)}) + (\Delta t)^2\mu\phi_{tt}^{n+(2/3)} \tag{15c}$$

The validity of the above three equations is subject to the condition given below

$$\phi^{n+1} = \phi^n + \Delta t\phi_t^n + \frac{(\Delta t)^2}{2!}\phi_{tt}^n + \frac{(\Delta t)^3}{3!}\phi_{ttt}^n + \frac{(\Delta t)^4}{4!}\phi_{tttt}^n + \cdots + \text{HOT} \tag{16}$$

The time derivatives are replaced with the spatial derivatives using the same idea described earlier. We are led to obtain $\alpha = \frac{-1}{32}$, $\beta = \frac{9}{8}$, $\gamma = \frac{-3}{32}$ and $\mu = \frac{3}{16}$ after some algebra. The derived three CDR equations given below can render fourth-order temporal accuracy

$$\bar{u}\phi_x^{n+(1/3)} - \bar{k}\phi_{xx}^{n+(1/3)} + 6\phi^{n+(1/3)} = \overline{f}^{n+(1/3)} + 6\phi^n + (\overline{f}^n - \bar{u}\phi_x^n + \bar{k}\phi_{xx}^n) + \frac{(\Delta t)^2}{3}\text{CT}_1 \tag{17a}$$

$$\bar{u}\phi_x^{n+(2/3)} - \bar{k}\phi_{xx}^{n+(2/3)} + 3\phi^{n+(2/3)} = \overline{f}^{n+(2/3)} + 3\phi^n + (\overline{f}^n - \bar{u}\phi_x^n + \bar{k}\phi_{xx}^n) + \frac{2(\Delta t)^2}{3}\text{CT}_2 \tag{17b}$$

$$\begin{aligned}\bar{u}\phi_x^{n+1} - \bar{k}\phi_{xx}^{n+1} + \frac{16}{9}\phi^{n+1} &= \overline{f}^{n+1} + \frac{16}{9}\phi^n - \frac{1}{18}(\overline{f}^n - \bar{u}\phi_x^n + \bar{k}\phi_{xx}^n) + 2(\overline{f}^{n+(1/3)} - \bar{u}\phi_x^{n+(1/3)} + \bar{k}\phi_{xx}^{n+(1/3)}) \\ &\quad - \frac{7}{6}(\overline{f}^{n+(2/3)} - \bar{u}\phi_x^{n+(2/3)} + \bar{k}\phi_{xx}^{n+(2/3)}) + \frac{(\Delta t)^2}{3}\text{CT}_3\end{aligned} \tag{17c}$$

where the correction terms CT_i $(i = 1-3)$ are written as

$$\text{CT}_1 = \frac{18}{(\Delta t)^2}(\phi^{n+(1/3)} - \phi^n) - \frac{3}{\Delta t}(\phi_t^{n+(1/3)} + \phi_t^n)$$

$$\text{CT}_2 = \frac{9}{2(\Delta t)^2}(\phi^{n+(2/3)} - \phi^n) - \frac{3}{2\Delta t}(\phi_t^{n+(2/3)} + \phi_t^n)$$

$$\text{CT}_3 = \frac{16}{3(\Delta t)^2}(\phi^{n+1} - \phi^n) + \frac{1}{6\Delta t}(\phi_t^n - 36\phi_t^{n+(1/3)} + 21\phi_t^{n+(2/3)} - 18\phi_t^{n+1})$$

4. SPATIAL DISCRETIZATION METHOD

The importance of approximating the one-dimensional convection–diffusion-reaction equation given below becomes apparent in view of Equations (10), (14) and (17)

$$u\phi_x - k\phi_{xx} + c\phi = f \tag{18}$$

We employ the general solution, which involves two constants c_1 and c_2, for Equation (18) to obtain a higher prediction accuracy

$$\phi = c_1 e^{\lambda_1 x} + c_2 e^{\lambda_2 x} + \frac{f}{c} \tag{19}$$

Substituting Equation (19) into Equation (18), we are led to obtain the following expressions for λ_1 and λ_2:

$$\lambda_1 = \frac{u + \sqrt{u^2 + 4ck}}{2k} \quad \text{and} \quad \lambda_2 = \frac{u - \sqrt{u^2 + 4ck}}{2k} \tag{20}$$

Using the operators similar to the central difference operators, the following discrete equation, which the analytic solution satisfies exactly provided that f is analytically prescribed, can be derived

$$\frac{u}{2h}(\phi_{i+1} - \phi_{i-1}) - \frac{m}{h^2}(\phi_{i+1} - 2\phi_i + \phi_{i-1}) + \frac{c}{6}(\phi_{i+1} + 4\phi_i + \phi_{i-1}) = f \tag{21}$$

In the above, h denotes the mesh size. By substituting the exact expressions for $\phi_i = c_1 e^{\lambda_1 x_i} + c_2 e^{\lambda_2 x_i} + (f/c)$, $\phi_{i+1} = c_1 e^{\lambda_1 h} e^{\lambda_1 x_i} + c_2 e^{\lambda_2 h} e^{\lambda_2 x_i} + (f/c)$, and $\phi_{i-1} = c_1 e^{-\lambda_1 h} e^{\lambda_1 x_i} + c_2 e^{-\lambda_2 h} e^{\lambda_2 x_i} + (f/c)$ into Equation (21), we can analytically derive m as

$$m = h^2 \left\{ \frac{\frac{c}{3} + \frac{c}{6}\cosh(\overline{\lambda_1})\cosh(\overline{\lambda_2}) + \frac{u}{2h}\sinh(\overline{\lambda_1})\cosh(\overline{\lambda_2})}{\cosh(\overline{\lambda_1})\cosh(\overline{\lambda_2}) - 1} \right\} \tag{22}$$

where

$$\overline{\lambda_1} = \frac{uh}{2k} \quad \text{and} \quad \overline{\lambda_2} = \sqrt{\left(\frac{uh}{2k}\right)^2 + \frac{ch^2}{k}} \tag{23}$$

Note that use of m given in Equation (22) can avoid the complex variable problem encountered in our previous article [3].

The present scheme involves calculating $\phi_x (\equiv Fh)$ and $\phi_{xx} (\equiv Gh^2)$ shown on the right-hand sides of Equations (10), (14) and (17). Our strategy is to calculate them implicitly from the two equations given, respectively, below

$$\alpha_0 F_{j+1} + \beta_0 F_j + \gamma_0 F_{j-1} = a_0(\phi_{j+2} - \phi_{j+1}) + b_0(\phi_{j+1} - \phi_j) + c_0(\phi_j - \phi_{j-1}) + d_0(\phi_{j-1} - \phi_{j-2}) \tag{24}$$

and

$$\alpha_1 G_{j+1} + \beta_1 G_j + \gamma_1 G_{j-1} = a_1 \phi_{j+2} + b_1 \phi_{j+1} + c_1 \phi_j + d_1 \phi_{j-1} + e_1 \phi_{j-2} \tag{25}$$

Note that approximation of ϕ_x and ϕ_{xx} with the sixth-order accuracy can be obtained provided that $(\alpha_0, \beta_0, \gamma_0, a_0, b_0, c_0, d_0) = (\frac{1}{5}, \frac{3}{5}, \frac{1}{5}, \frac{1}{60}, \frac{29}{60}, \frac{29}{60}, \frac{1}{60})$ and $(\alpha_1, \beta_1, \gamma_1, a_1, b_1, c_1, d_1, e_1) = (1, \frac{11}{2}, 1, \frac{3}{8}, 6, -\frac{51}{4}, 6, \frac{3}{8})$.

This is followed by representing the implicit equations for F and G at nodal points immediately adjacent to the boundary points. Theoretically, it is legitimate to specify $d_0 = e_1 = 0$ and $a_0 = a_1 = 0$ at nodes immediately adjacent to the left and right boundaries, respectively. Use of the Taylor series expansion enables us to analytically derive $(\alpha_1, \beta_1, \gamma_1, a_1, b_1, c_1, d_1, e_1) = (1, 10, 1, 0, 12, -24, 12, 0)$. In addition, we can have $(\alpha_0, \beta_0, \gamma_0, a_0, b_0, c_0, d_0) = (\frac{3}{10}, \frac{3}{5}, \frac{1}{10}, \frac{1}{30}, \frac{19}{30}, \frac{1}{3}, 0)$ and $(\frac{1}{10}, \frac{3}{5}, \frac{3}{10}, 0, \frac{1}{3}, \frac{19}{30}, \frac{1}{30})$ at nodes next to the left and right boundaries, respectively.

5. THEORETICAL STUDY OF THE DISCRETIZATION SCHEME

Theoretical studies of the proposed schemes detailed in Sections 3 and 4 begin with deriving the following one-step equations, which are equivalent to those derived in Section 3:

One-step second-order scheme:

$$\phi^{n+1} = \phi^n + \frac{\Delta t}{2}(\phi_t^n + \phi_t^{n+1}) + \mathrm{CT}_1 \tag{26}$$

Two-step third-order scheme:

$$\phi^{n+1} = \phi^{n+(1/3)} + \frac{\Delta t}{12}(10\phi_t^n - 11\phi_t^{n+(1/3)} + 9\phi_t^{n+1}) + \mathrm{CT}_2 \tag{27}$$

Three-step fourth-order scheme:

$$\phi^{n+1} = \frac{1}{2}(\phi^{n+(1/3)} + \phi^{n+(2/3)}) + \frac{\Delta t}{96}(-27\phi_t^n + 100\phi_t^{n+(1/3)} - 79\phi_t^{n+(2/3)} + 54\phi_t^{n+1}) + \mathrm{CT}_3 \tag{28}$$

For the sake of simplicity, the analysis will be performed at the one-dimensional limiting case for revealing the schemes' dissipative and dispersive natures for the following equation:

$$\phi_t + u\phi_x - k\phi_{xx} = 0 \tag{29}$$

Subject to the initial condition given by $\phi(x, t=0) = \exp(\mathrm{i}k_m x)$, Equation (29) can be easily shown to have the exact solution given by

$$\phi(x,t) = \exp[-(kk_m^2 + c)t]\exp[\mathrm{i}k_m(x - ut)] \tag{30}$$

where k_m denotes the wave-number. With $h(\equiv \Delta x)$ chosen as the mesh size and Δt as the time increment, the discrete equation for (29) is as follows:

$$A_1\phi_{j-1}^{n+1} + A_2\phi_j^{n+1} + A_3\phi_{j+1}^{n+1} = \sum_{k=-4}^{3} B_k \phi_{j+k}^{n+r} \tag{31}$$

The tri-diagonal coefficients A_1, A_2 and A_3 shown above are expressed in terms of $v = u\Delta t/h$ as

$$A_{1,3} = \mp\frac{v}{2} - \overline{m} - \frac{c}{6} \tag{32a}$$

$$A_2 = 2\overline{m} + \frac{4c}{6} \tag{32b}$$

where c is the constant. According to the definition for $Pe(=uh/k)$, $\overline{m}$ shown in Equation (32) can be theoretically derived as

$$\overline{m} = h^2 \left\{ \frac{\frac{c}{3} + \frac{c}{6}\cosh(\overline{\lambda_1}^*)\cosh(\overline{\lambda_2}^*) + \frac{v}{2}\sinh(\overline{\lambda_1}^*)\cosh(\overline{\lambda_2}^*)}{\cosh(\overline{\lambda_1}^*)\cosh(\overline{\lambda_2}^*) - 1} \right\} \tag{33}$$

where $\overline{\lambda_1}^* = Pe/2$ and $\overline{\lambda_2}^* = [(Pe/2)^2 + (Pe/v)c]^{1/2}$.

Owing to the phase and amplitude errors introduced in the discretization, the exact solution to the discrete equation for (29) is assumed to take the following expression:

$$\phi(x,t) = \exp\left[-(kk_m^2 + c)\frac{k_r}{\alpha^2}t\right]\exp\left[\mathrm{i}k_m\left(x - u\frac{k_i}{\alpha}t\right)\right] \tag{34}$$

where $\alpha(\equiv k_m h)$ is the modified wave-number. Dispersion analysis of Equation (31) starts by substituting ϕ_j and $\phi_{j\pm1}$, which are obtained from Equation (34), into Equation (31). After some algebra, k_r and k_i accounting for the amplitude and phase errors are derived as

$$k_r = -\frac{p}{\left(\frac{v}{Pe} + \frac{c}{\alpha^2}\right)} \tag{35a}$$

$$k_i = -\frac{q}{v} \tag{35b}$$

where

$$p = \ln\left\{ \sqrt{\left(\frac{f_1 \cdot a - f_2 \cdot b}{a^2 + b^2}\right)^2 + \left(\frac{f_1 \cdot b + f_2 \cdot a}{a^2 + b^2}\right)^2} \right\} \tag{36a}$$

$$q = \tan^{-1}\left\{ \frac{f_1 \cdot b + f_2 \cdot a}{f_1 \cdot a - f_2 \cdot b} \right\} \tag{36b}$$

In the above two equations, a and b are derived as

$$a = (A_1 + A_3)\cos\alpha + A_2 \tag{37a}$$

$$b = (A_1 - A_3)\sin\alpha \tag{37b}$$

where f_1 and f_2 are shown in Appendix A.

For clearly revealing the dissipative and dispersive errors, we plot k_r and k_i against Pe and v. By virtue of Figures 1 and 2, which are plotted at $v = 0.2$ and 0.5, we are led to know that k_r and k_i agree perfectly with α^2 and α, respectively, in the small modified wave-number

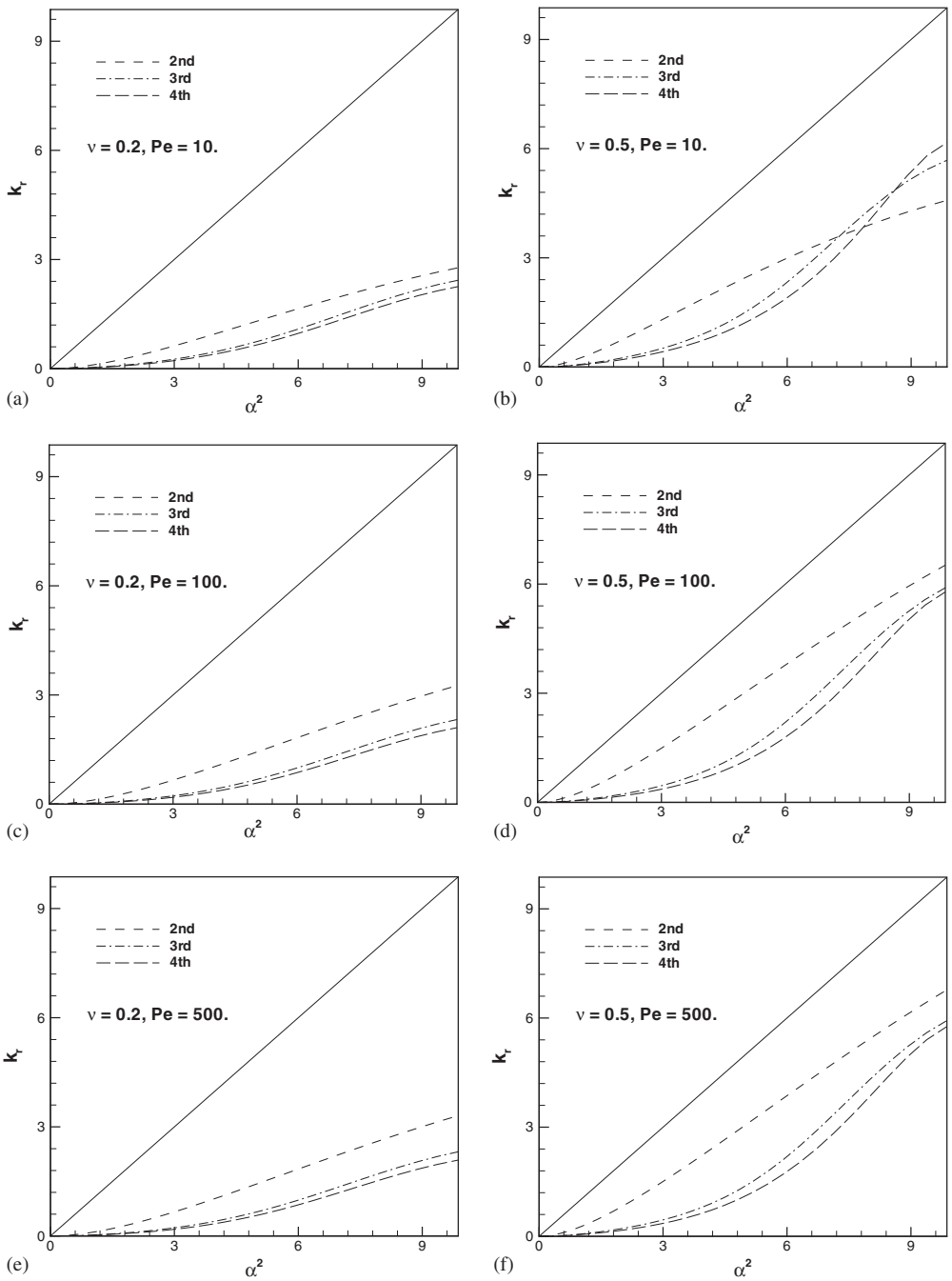

Figure 1. Plots of k_r against the modified wave-number α^2 for $v(=0.2, 0.5)$. The exact expression for k_r (solid line) is also plotted for the comparison purpose: (a)–(b) $Pe = 10$; (c)–(d) $Pe = 100$; and (e)–(f) $Pe = 500$.

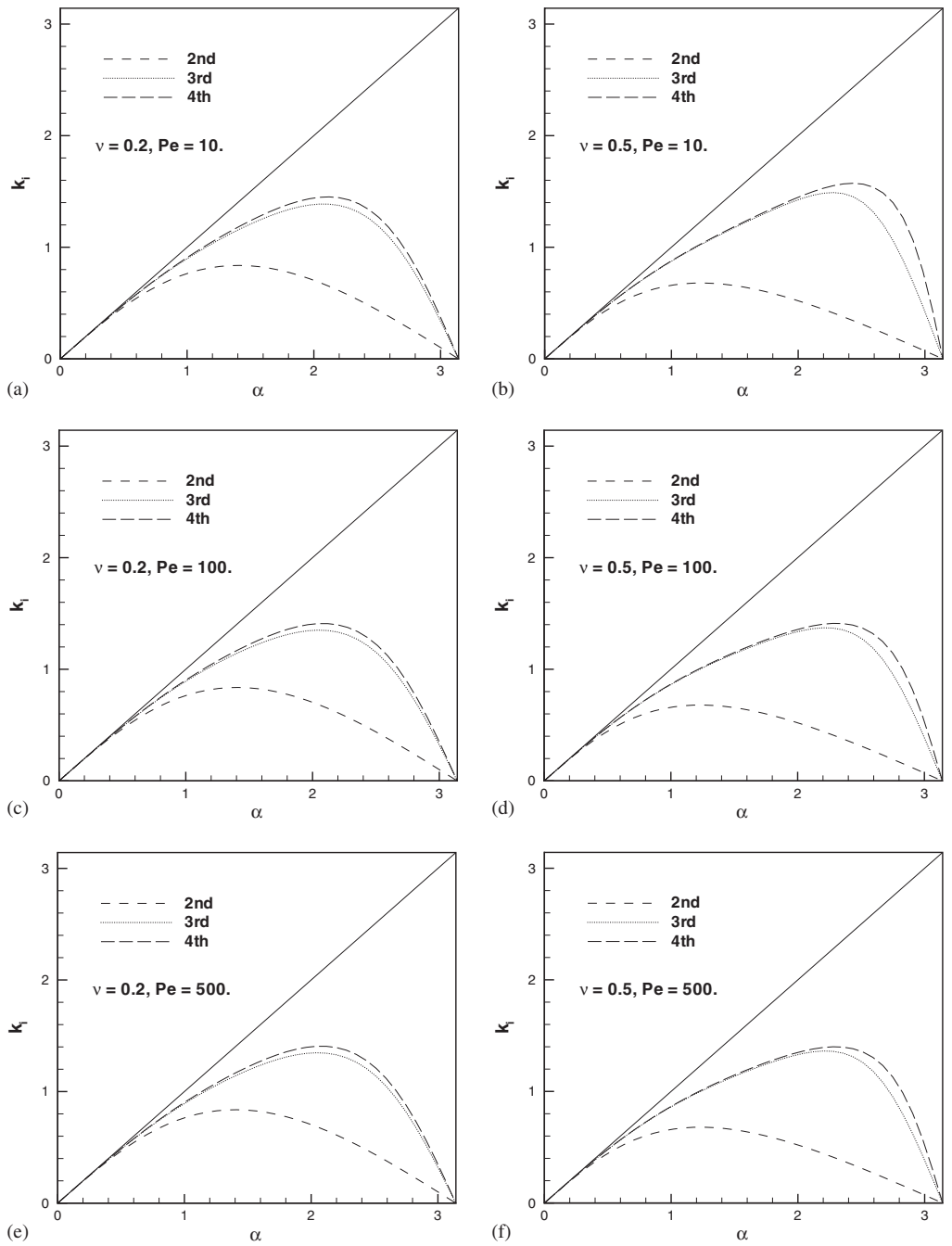

Figure 2. Plots of k_i against the modified wave-number α for $v(=0.2, 0.5)$. The exact expression for k_i (solid line) is also plotted for the comparison purpose: (a)–(b) $Pe = 10$; (c)–(d) $Pe = 100$; and (e)–(f) $Pe = 500$.

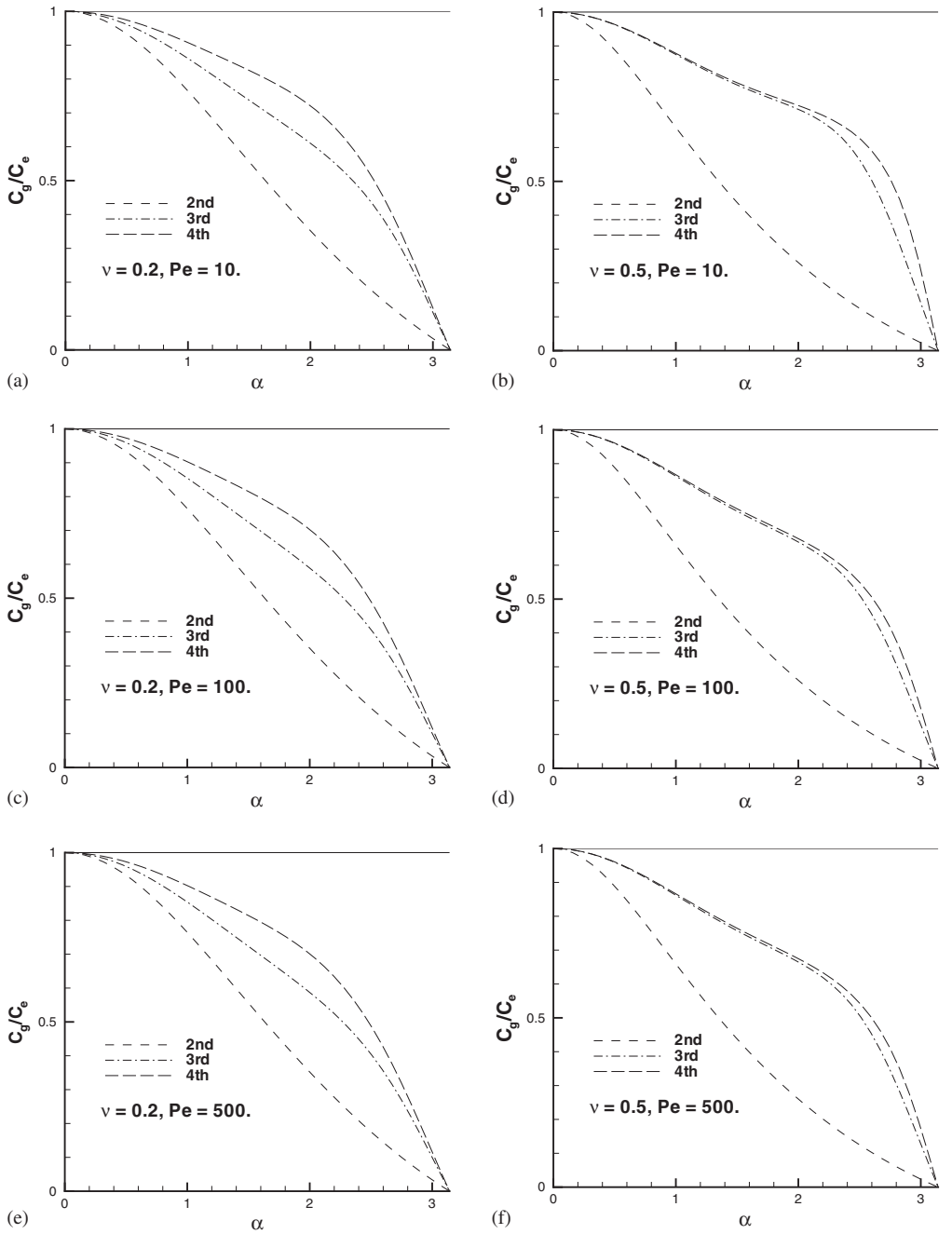

Figure 3. Plots of the group velocity ratio C_g/C_e against the modified wave-number α for $v(=0.2, 0.5)$. The exact ratio of group velocities (solid line) is also plotted for the comparison purpose: (a)–(b) $Pe = 10$; (c)–(d) $Pe = 100$; and (e)–(f) $Pe = 500$. Note that C_g and C_e are the numerical and exact group velocities, respectively.

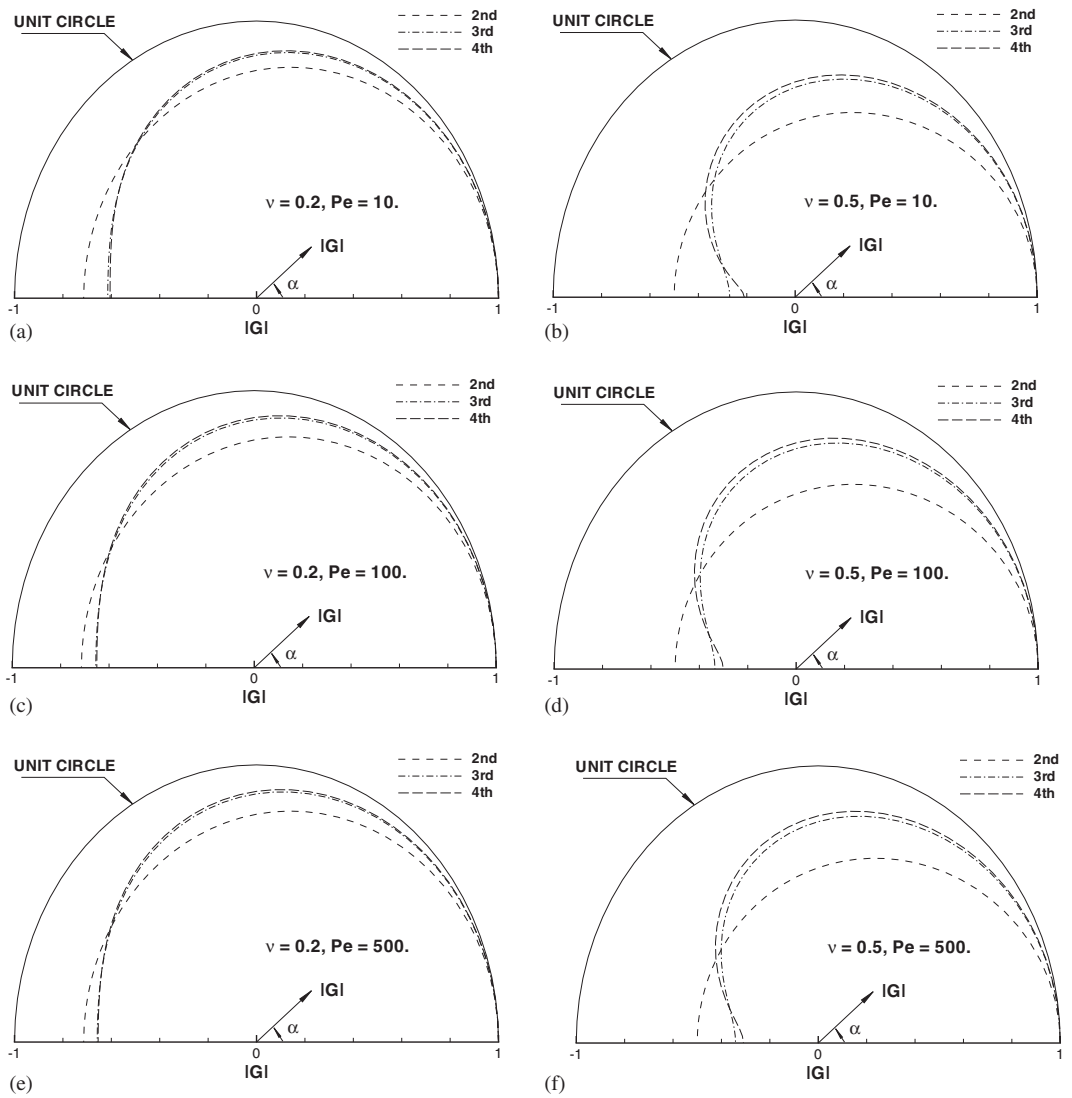

Figure 4. Plots of the amplification factor $|G|$ against the modified wave-number α for $v(=0.2, 0.5)$: (a)–(b) $Pe = 10$; (c)–(d) $Pe = 100$; and (e)–(f) $Pe = 500$.

range. The higher the modified wave-number, the less satisfactory agreement is seen to occur. Note that the proposed scheme is dissipative since $k_r > 0$ in the entire wave-number range. In Figure 3, the numerical group velocity $C_g(\equiv (\mathrm{d}w/\mathrm{d}k_m))$, where w is obtained from the dispersion relation, is observed to have a magnitude smaller than the analytical propagation speed. The proposed scheme is, thus, classified to be phase-lagging.

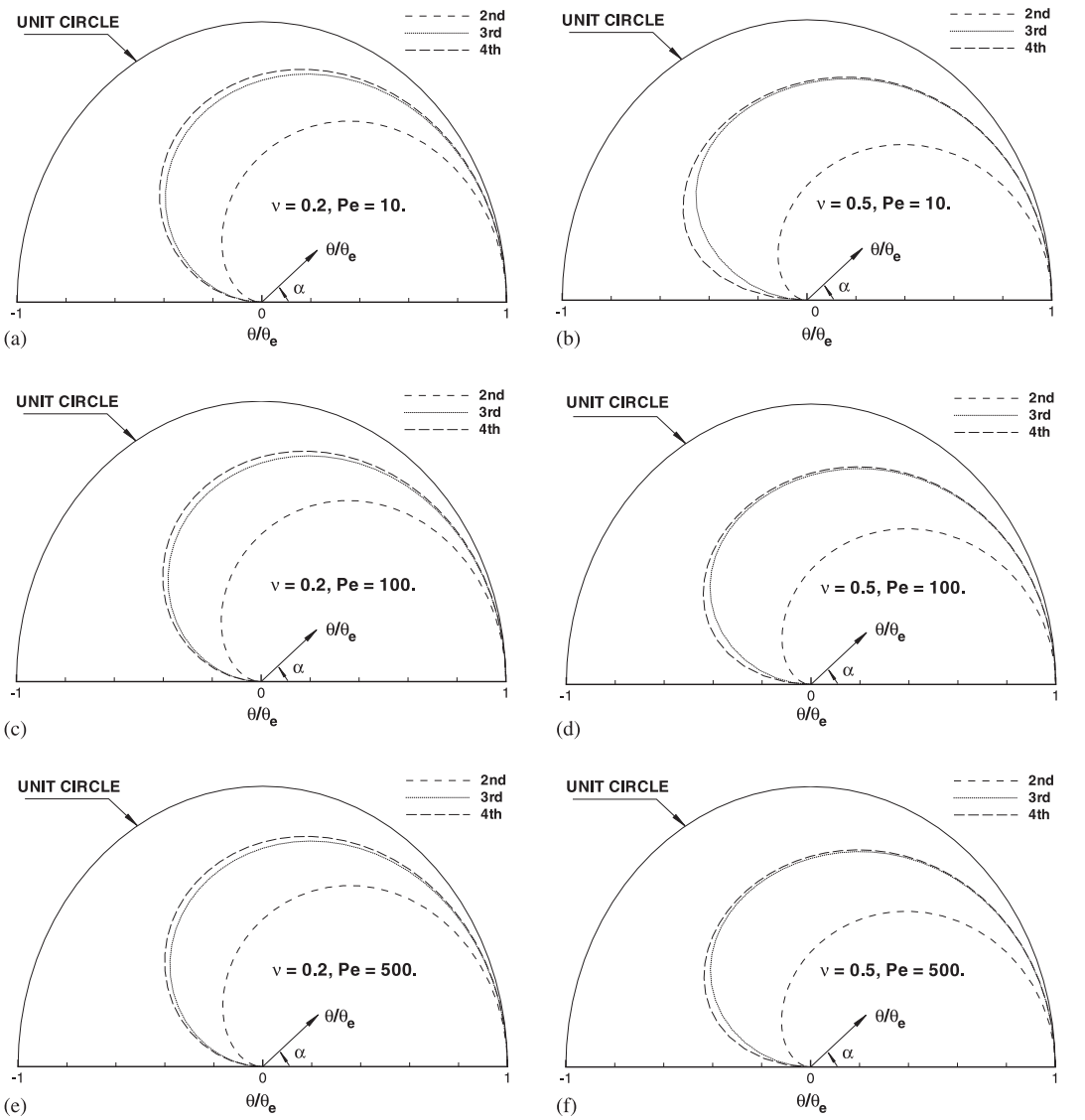

Figure 5. Plots of the phase angle ratio θ/θ_e against the modified wave-number α for $\nu(=0.2, 0.5)$: (a)–(b) $Pe=10$; (c)–(d) $Pe=100$; and (e)–(f) $Pe=500$.

We also conduct Fourier (or von Neumann) stability analysis [4, 5] to reveal the schemes' amplification factors. Let $\alpha=(2\pi m/2L)h$ $(m=0,1,2,3,\ldots M)$, h being the grid size, and $2L$ being the period of fundamental frequency $(m=1)$, the magnitude of amplification factor $|G|(\equiv|\phi_j^{n+1}/\phi_j^n|)$ can be derived in terms of p and q given in Equations (36a) and (36b), where

$$G=\mathrm{e}^p(\cos q+\mathrm{i}\sin q) \tag{38}$$

In view of Figure 4, the proposed scheme is unconditionally stable. The amplification factor shown above can be rewritten in its exponential form as $G = |G|\ e^{i\theta}$, where the phase angle θ is defined as

$$\theta = \tan^{-1}\left|\frac{\mathrm{Im}(G)}{\mathrm{Re}(G)}\right| \tag{39}$$

To study how θ varies with $Pe = uh/k$ and $v = u\Delta t/h$, we need to derive the exact phase angle θ_e, which is $-v\alpha$. The ratio θ/θ_e is plotted in terms of α in Figure 5.

6. NUMERICAL RESULTS

6.1. *Validation of the theoretical rates of convergence*

As a first step towards validating the theoretical rates of convergence for the proposed two-dimensional schemes, we consider Equation (29) in $0 \leqslant x \leqslant 1$ at $k = 1$. Subject to the

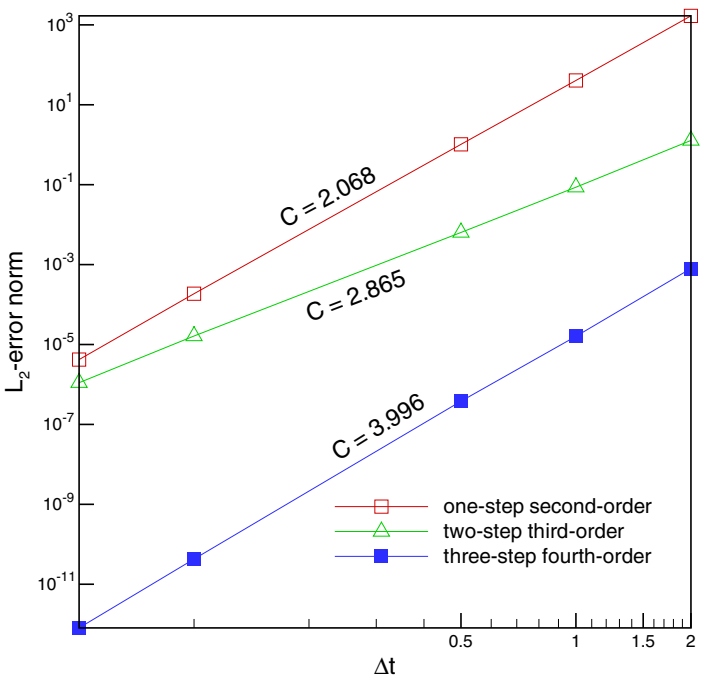

Figure 6. The simulated temporal rates of convergence **C** ('□' for the one-step second-order time-stepping scheme; '△' for the two-step third-order time-stepping scheme; '■' for the three-step fourth-order time-stepping scheme) for the one-dimensional problem considered in Section 6.1. Note that the current error norms were obtained at $t = 4$.

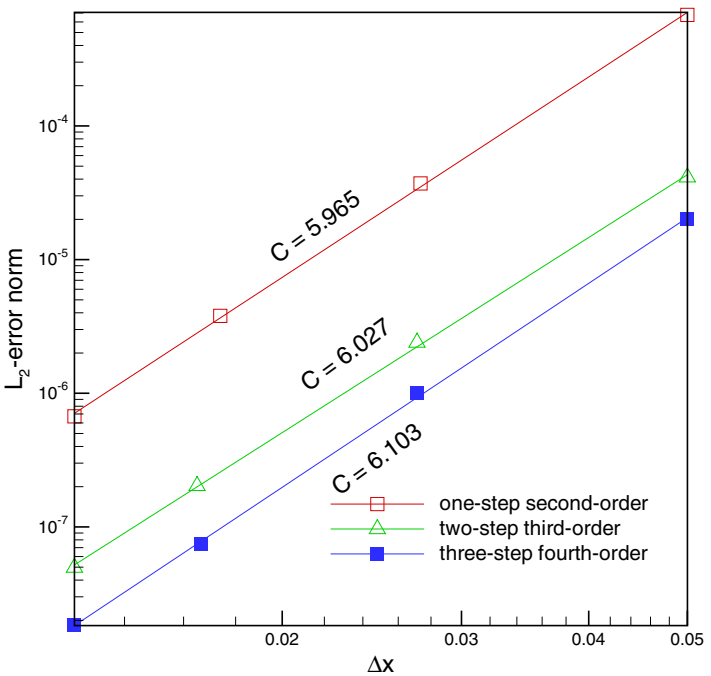

Figure 7. The simulated spatial rates of convergence **C** for the one-dimensional problem considered in Section 6.1 using the proposed time-stepping schemes ('□' for the one-step second-order time-stepping scheme; '△' for the two-step third-order time-stepping scheme; '■' for the three-step fourth-order time-stepping scheme). Note that the current error norms were obtained at $t = 1$.

prescribed initial condition

$$\phi(x,0) = \frac{\frac{\pi}{2}\sin(\pi x) + 2\pi\sin(2\pi x)}{1 + \frac{1}{4}\cos(\pi x) + \frac{1}{2}\cos(2\pi x)}$$

and the boundary conditions $\phi(0,t) = \phi(1,t) = 0$, Equation (4) is amenable to the following analytic solution [6]:

$$\phi(x,t) = \frac{\frac{\pi}{2}[\exp(-\pi^2 t)\sin(\pi x) + 4\exp(-4\pi^2 t)\sin(2\pi x)]}{1 + \frac{1}{4}\exp(-\pi^2 t)\cos(\pi x) + \frac{1}{2}\exp(-4\pi^2 t)\cos(2\pi x)} \tag{40}$$

In what follows, the specified tolerance, cast in the L_2-norm form, mentioned in Section 3 is 10^{-12} for ϕ obtained at two consecutive iterations. Computations were carried out at Δt $(= 2, 1, \frac{1}{2}, \frac{1}{10}, \frac{1}{20}, \frac{1}{100})$ and $\Delta x = 10^{-3}$. The predicted L_2-error norms at $t = 4$ were employed to plot $\log(\frac{\mathrm{err}_1}{\mathrm{err}_2})$ against $\log(\frac{\Delta t_1}{\Delta t_2})$, where err_1 and err_2 were computed at two consecutively refined time-steps Δt_1 and Δt_2. As seen in Figure 6, the computed temporal rates of convergence for three investigated schemes agree approximately with their respective theoretical

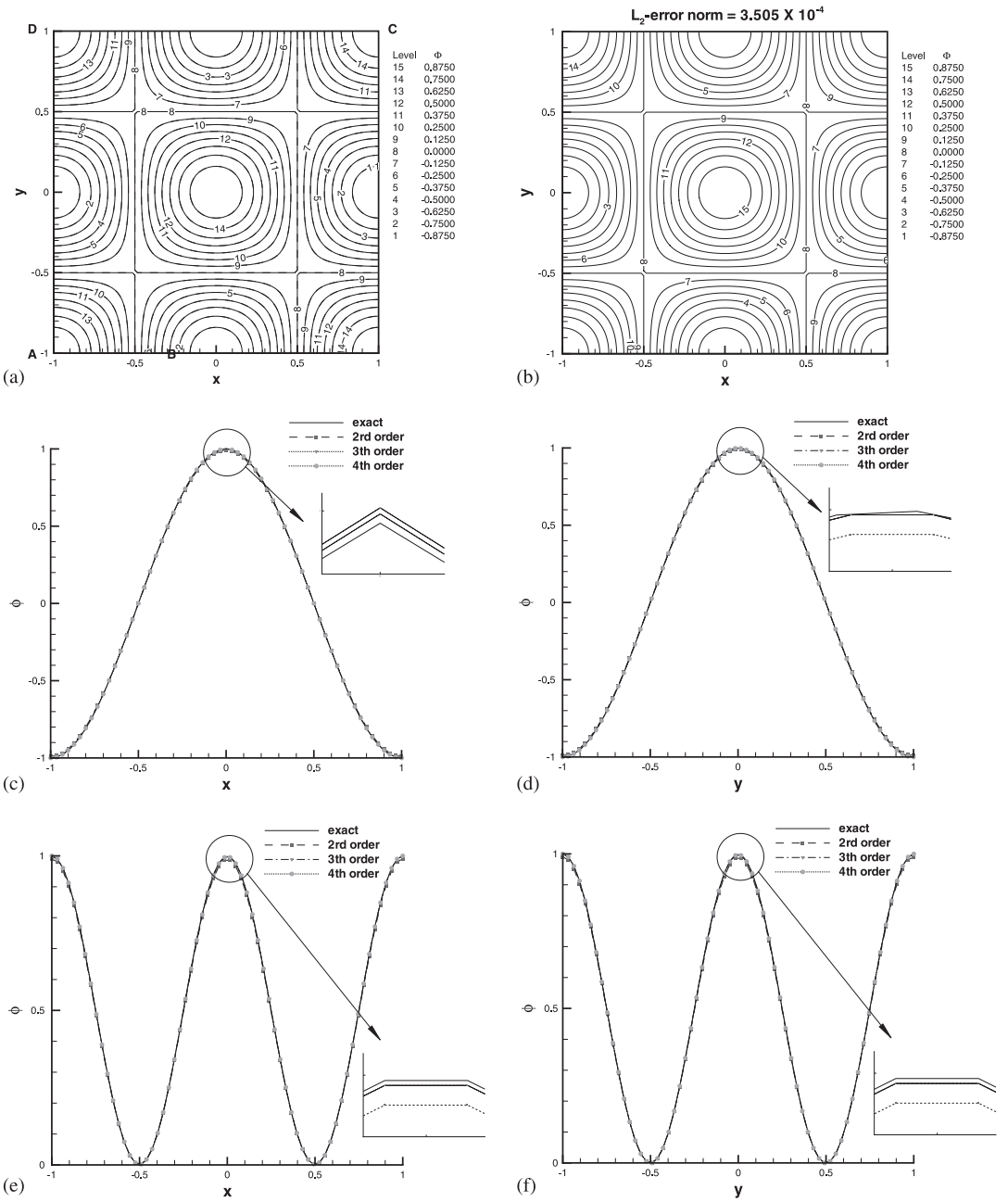

Figure 8. The solution computed at $t = 1$ for the two-dimensional problem given in Section 6.1: (a) exact contours; (b) computed contours; (c) the computed ϕ along $\overline{AB}$; (d) the computed ϕ along $\overline{AD}$; (e) the computed ϕ along $\overline{AC}$; and (f) the computed ϕ along $\overline{BD}$.

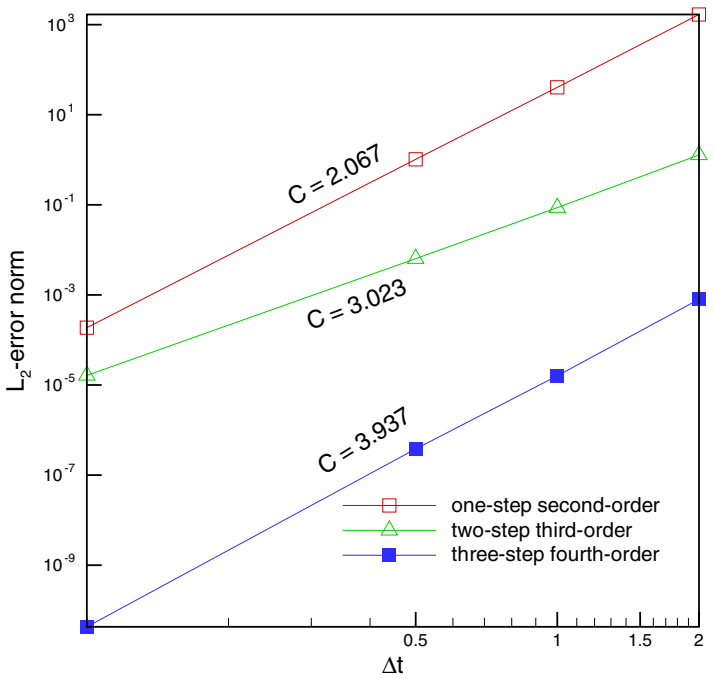

Figure 9. The simulated temporal rates of convergence **C** for the two-dimensional problem considered in Section 6.1. ('□' for the one-step second-order time-stepping scheme; '△' for the two-step third-order time-stepping scheme; '■' for the three-step fourth-order time-stepping scheme). Note that the L_2-error norms were obtained at $t = 4$.

orders. For the sake of completeness, we also plot in Figure 7 the spatial rates of convergence based on the solutions obtained at $\Delta x = \frac{1}{5}, \frac{1}{10}, \frac{1}{20}, \frac{1}{40}, \frac{1}{80}$ and $\Delta t = 10^{-4}$. The simulated spatial rates of convergence are all found to be slightly different from the theoretical rate, namely, 6.

We will then demonstrate that the proposed CDR scheme, applied together with the alternating direction implicit solution algorithm, for the two-dimensional convection–diffusion equation can also render the theoretical rates. Subject to the following initial condition:

$$\phi(x, y, t = 0) = \cos(\pi x)\cos(\pi y) \tag{41}$$

Equation (1) is solved in a square $0 \leqslant x, y \leqslant 1$ at $k = 10^{-3}$ and the prescribed velocity field $(u, v) = (-\pi\cos(\pi x)\sin(\pi y)\exp(-2k\pi^2 t),\ \pi\sin(\pi x)\cos(\pi y)\exp(-2k\pi^2 t))$. This problem is amenable to the following exact solution:

$$\phi(x, y, t) = \cos(\pi x)\cos(\pi y)\exp(-2k\pi^2 t) \tag{42}$$

The integrity of the proposed two-dimensional scheme, calculated at $\Delta x = \Delta y = \frac{1}{64}$ and $\Delta t = 10^{-3}$, can be clearly demonstrated in Figure 8.

As seen in Figure 9, the computed temporal rates of convergence for three schemes investigated at $\Delta x = \Delta y = 10^{-3}$ and $\Delta t = 2, 1, \frac{1}{5}, \frac{1}{10}, \frac{1}{20}, \frac{1}{100}$ agree well with their respective theoretical

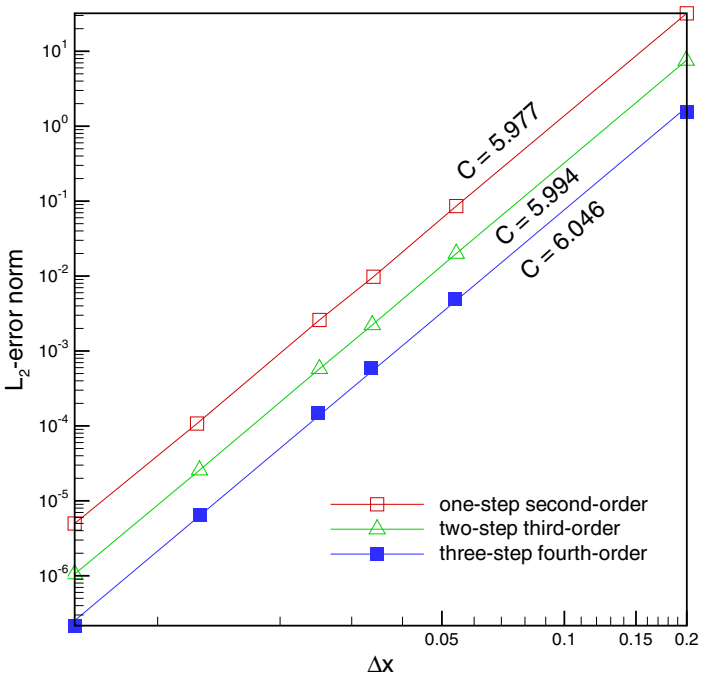

Figure 10. The simulated spatial rates of convergence **C** for the two-dimensional problem considered in Section 6.1 using the proposed time-stepping schemes ('□' for the one-step second-order time-stepping scheme; '△' for the two-step third-order time-stepping scheme; '■' for the three-step fourth-order time-stepping scheme). Note that the L_2-error norms were obtained at $t = 1$.

orders. For the sake of completeness, we also plot in Figure 10 the spatial rates of convergence using the solutions obtained at $\Delta x = \Delta y = \frac{1}{5}, \frac{1}{10}, \frac{1}{20}, \frac{1}{40}, \frac{1}{80}, \frac{1}{160}$ and $\Delta t = 10^{-4}$. The simulated spatial rates of convergence are all found to be close to 6, which is the theoretical rate of convergence.

6.2. *Two-dimensional sharply varying unsteady CD equation*

The final test problem considers the mixing of two fluids of different concentrations ϕ in a square $-4 \leqslant x, y \leqslant 4$. Our aim is to check whether the discretization scheme can capture the evolving high concentration gradient. Initially, ϕ is set at

$$\phi(x, y, t = 0) = -\tanh\left(\frac{y}{2}\right) \tag{43}$$

Subsequent to $t = 0$, ϕ will be varied with the velocity field given by $u(x, y) = -\overline{T}(y/r)$ and $v(x, y) = \overline{T}(x/r)$. In the above equation, $\overline{T}$ denotes the ratio of tangential velocity at a location, which is apart from $(0, 0)$ with a distance of r, and its maximum velocity

$$\overline{T} = \frac{\operatorname{sech}^2 r \tanh r}{\max[\operatorname{sech}^2 r \tanh r]} \tag{44}$$

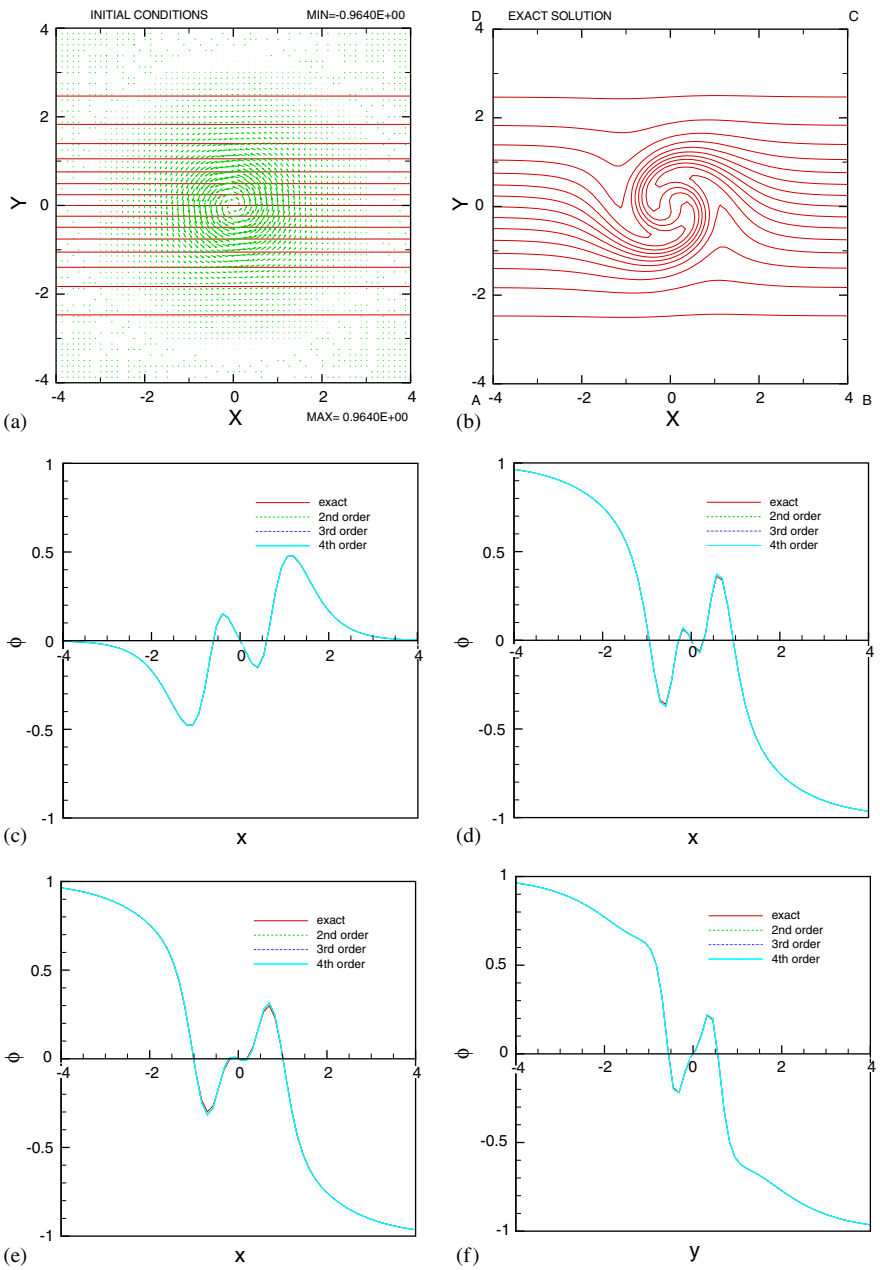

Figure 11. The simulated solutions for solving the problem, given in Section 6.2, which represents the mixing of fluid flows with high and low concentrations: (a) initial condition; (b) the exact ϕ contours for the inviscid case; (c) the solution computed along $y = 0$; (d) the solution computed along $\overline{AC}$; (e) the solution computed along $x = 0$; and (f) the solution computed along $\overline{BD}$.

In the present computation, the number of grid points is 160×160, thereby yielding the constant mesh size $\Delta x = \Delta y = 0.05$. Figure 11 shows $\phi(x, y, t = 5.0)$ computed at $k = 10^{-10}$. The sharply changing concentration profile at $t = 0$ is seen to be twisted by the specified flow field and is gradually developed to show a spiral-type distribution. For the sake of comparison, we also plot in Figure 11 the exact solution at the limiting condition $k = 0$ [7, 8]

$$\phi(x, y, t) = -\tanh\left[\frac{y}{2}\cos(wt) - \frac{x}{2}\sin(wt)\right] \tag{45}$$

In the above, $w = \overline{T}/r$ denotes the rotation frequency.

7. CONCLUDING REMARKS

The aim of this study is to develop three schemes with the temporal accuracy orders of 2, 3 and 4 for solving the two-dimensional unsteady convection–diffusion transport equation. Our strategy is to transform the unsteady convection–diffusion equation to the steady convection–diffusion-reaction equation. The key to success in solving the investigated two-dimensional transport equation lies in the developed convection–diffusion-reaction scheme. In this study, we have developed a nodally exact one-dimensional CDR scheme so that the prediction error stems primarily from the employed temporal discretization schemes. In the replacement of the time derivative terms with the spatial derivative terms, we avoid invoking the spatial derivatives having orders higher than 2. A full assessment of the proposed schemes requires a rigorous test. For this reason, we perform the fundamental studies for three investigated schemes and solve the problems that are all amenable to the exact solutions. Based on the computed L_2-error norms and the resulting rates of convergence, the proposed advection–diffusion schemes are validated. The problem with high-gradient solution profile is also investigated. Good ability to capture the sharply varying solution has been demonstrated.

APPENDIX A

The coefficients f_1 and f_2 shown in Equations (36a) and (36b) are given below

One-step second-order scheme:

$$f_1 = 2 - \frac{v}{60}k_1 + \frac{v}{180Pe}k_2 \tag{A1}$$

$$f_2 = \frac{v}{60}k_3 \tag{A2}$$

Two-step third-order scheme:

$$f_1 = \frac{4}{3}\left[1 - \frac{v}{60}k_1 + \frac{v}{180Pe}k_2\right] + e^{1/3p}\left[\frac{v}{60}\left(k_1\cos\frac{1}{3}q + k_3\sin\frac{1}{3}q\right) - \frac{v}{180Pe}k_2\cos\frac{1}{3}q\right] \tag{A3}$$

$$f_2 = \frac{4}{3}\frac{v}{60}k_3 + e^{1/3p}\left[\frac{v}{60}\left(k_1\sin\frac{1}{3}q - k_3\cos\frac{1}{3}q\right) - \frac{v}{180Pe}k_2\sin\frac{1}{3}q\right] \tag{A4}$$

Three-step fourth-order scheme:

$$f_1 = \frac{1}{18}\left(\frac{v}{60}k_1 - \frac{v}{180Pe}k_2\right) - 2e^{1/3p}\left[\frac{v}{60}\left(k_1\cos\frac{1}{3}q + k_3\sin\frac{1}{3}q\right) - \frac{v}{180Pe}k_2\cos\frac{1}{3}q\right] + \frac{7}{6}e^{2/3p}\left[\frac{v}{60}\left(k_1\cos\frac{2}{3}q + k_3\sin\frac{2}{3}q\right) - \frac{v}{180Pe}k_2\cos\frac{2}{3}q\right] \tag{A5}$$

$$f_2 = -\frac{1}{18}\frac{v}{60}k_3 - 2e^{1/3p}\left[\frac{v}{60}\left(k_1\sin\frac{1}{3}q - k_3\cos\frac{1}{3}q\right) - \frac{v}{180Pe}k_2\sin\frac{1}{3}q\right] + \frac{7}{6}e^{2/3p}\left[\frac{v}{60}\left(k_1\sin\frac{2}{3}q - k_3\cos\frac{2}{3}q\right) - \frac{v}{180Pe}k_2\sin\frac{2}{3}q\right] \tag{A6}$$

where

$$k_1 = \cos 4\alpha - 8\cos 3\alpha + 28\cos 2\alpha - 56\cos\alpha + 35 \tag{A7}$$

$$k_2 = 4\cos 3\alpha - 54\cos 2\alpha + 540\cos\alpha - 490 \tag{A8}$$

$$k_3 = \sin 4\alpha - 8\sin 3\alpha + 32\sin 2\alpha - 104\sin\alpha \tag{A9}$$

ACKNOWLEDGEMENTS

We would like to acknowledge the financial support from National Science Council under NSC 92-2611-E-002-008. This work was partially accomplished in the course of the second author's sabbatical leave in University of Paris 6. Excellent research resources provided by professors Oliver Pironneau and Yvon Maday are highly appreciated.

REFERENCES

1. Patankar SV. *Numerical Heat Transfer and Fluid Flow*. Washington, 1980.
2. Peaceman DW, Rachford HH. The numerical solution of parabolic and elliptic differential equations. *Journal of the Society for Industrial and Applied Mathematics* 1955; **3**:28–41.
3. Sheu TWH, Wang SK, Lin RK. An implicit scheme for solving the convection–diffusion-reaction equation in two dimensions. *Journal of Computational Physics* 2000; **164**:123–142.
4. Richtmyer RD, Morton KW. *Difference Methods for Initial Value Problems*. Interscience Publishers/Wiley: New York, 1967.
5. von Neumann J, Richtmyer RD. A method for the numerical calculation on hydrodynamic shock. *Journal of Applied Physics* 1950; **21**:232–237.
6. Cole JD. On a quasilinear equation occurring in aerodynamics. *Quarterly Journal of Mechanics and Applied Mathematics* 1951; **9**:225–236.
7. Tamamidis P, Assanis DN. Evaluation for various high-order-accuracy schemes with and without flux limiters. *International Journal for Numerical Methods in Fluids* 1993; **16**:931–948.
8. Doswell CA. A kinematic analysis of frontogenesis associated with a nondivergent vortex. *Journal of Atmospheric Sciences* 1984; **41**:1242–1248.

